Journal of Power Sources 191 (2009) 456–464

Contents lists available at ScienceDirect

Journal of Power Sources

journal homepage: www.elsevier.com/locate/jpowsour

Analysis of the diffusive mass transport in the anode side porous backing layer of a direct methanol fuel cell

Matthias Möst[a], Matthias Rzepka[a,*], Ulrich Stimming[a,b]

[a] ZAE Bayern, Division 1, 85748 Garching, Germany
[b] TU München, Department of Physics E19, 85748 Garching, Germany

ARTICLE INFO

Article history:
Received 8 December 2008
Received in revised form 11 February 2009
Accepted 14 February 2009
Available online 28 February 2009

Keywords:
Gas diffusion layer
Mass transport
Effective transport coefficient
Tortuosity
DMFC
Random walk simulation

ABSTRACT

In this work we present an analysis of the mass transport in the anode side porous backing layer of a direct methanol fuel cell (DMFC). The effective transport coefficient of different backing layers at various compressions was measured and compared to two different literature models and a single particle random walk simulation which accounts for details of the geometrical fibre microstructure. Based on the measured values of the effective transport coefficient limiting current densities for diffusive transport were calculated taking into account geometric boundary conditions and anisotropic and inhomogeneous backing layer properties. Comparison with the measured values for the limiting current in fuel cell operation shows qualitative agreement. A systematic underestimation indicates that also other transport processes contribute significantly to the mass transfer at the used experimental setup.

1. Introduction

A direct methanol fuel cell (DMFC) is an electrochemical device that converts chemical energy into electrical energy. The DMFC assembly is shown in Fig. 1. The reactants, a methanol water solution on the anode side and oxygen in pure form or as part of air on the cathode side, are supplied to the cell via a flow field with a channel-rib structure. From the channels of the flow field the reactants are transported through the porous backing layer to the electrodes where the reactions take place. The role of the flow field ribs is to transport the released electrons to the external circuit. The electronic non-conducting polymer electrolyte membrane (PEM) serves as exchange medium for protons between anode and cathode electrode.

The porous backing layer (BL), often denoted as (gas) diffusion layer, plays an important role in the DMFC setup. First of all it provides, referring to Fig. 2, access for the reactants to the area under the flow field ribs. In addition the BL has to enable the removal of the reaction products. Further it electronically connects the electrode areas under the flow field channels to the flow field ribs. Therefore, a backing layer material has to be porous to combine electronic conductivity and mass transport.

Materials made of carbon fibres match the requirements in a DMFC to a good extend. A detailed overview over backing layer materials is given in [1].

For H_2-PEM fuel cells usually similar backing layers are used. Hence, there are many publications to characterise backing layer properties and to find connections to the mass transport behaviour. Mathias et al. [1] also gives a good survey of the different characterisation methods. For ex situ characterisations the porosity and pore size distribution [2,3], various types of permeability [3–6] and liquid–surface interactions [3,7,8] are measured. Kramer et al. [9] and Baker et al. [10] introduce two different techniques to measure the effective transport coefficient.

For an in situ analysis of the mass transport behaviour of the BL limiting current measurements are used. Xu et al. [11] shows for the DMFC the overall mass transfer coefficients at various flow rates with two different flow field geometries. Scott et al. [12] give the mass transfer coefficient at various methanol concentrations and temperatures.

Studies to find interconnections between ex situ and in situ measurements for the H_2-PEM fuel cell have been reported [2,3,10]. Ihonen et al. [2] tried to link the cell performance under two-phase conditions to porosity and pore size distribution. Willimas et al. [3] found an empirical correlation between the gas permeability perpendicular to the cathode side backing layer plane and the limiting current. No connection of the fraction of hydrophobic pores and porosity to the in situ measurements could be shown. Baker et al. [10] compared the measurements of the effective diffusivity of the

* Corresponding author. Tel.: +49 89 329442 31; fax: +49 89 329442 12.
E-mail address: rzepka@muc.zae-bayern.de (M. Rzepka).

0378-7753/$ – see front matter © 2009 Elsevier B.V. All rights reserved.
doi:10.1016/j.jpowsour.2009.02.037

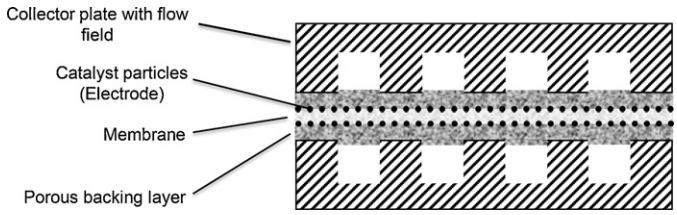

Fig. 1. Schematic design of the direct methanol fuel cell. The reactants are supplied via the flow field channels and transported through the porous backing layer to the electrode where the reaction takes place. The collector plates are connected to an external circuit.

BL in a diffusion cell with limiting current measurements and found good agreement.

In this work an analysis of the diffusive mass transport of methanol on the anode side of a DMFC is presented. We show that the effective transport coefficient of the porous backing layer has a major influence on limiting current density. Therefore, the effective transport coefficient of various materials is measured with the method developed in [9]. The results of these measurements are compared via a simple model equation and a Monte Carlo simulation of the diffusion process with the experimental determined limiting currents. Further the correlation between tortuosity and porosity has been analysed for different BLs at various compressions and compared with model equations. A Monte Carlo simulation was used to study the influence of different microstructures on the diffusion process.

2. Theory

2.1. Model for the methanol transport

In order to analyse the influence of backing layer parameters on the mass transport on the anode side of a DMFC a simple theoretical model equation has been set up. In general, the cell voltage decreases with increasing current density due to several loss mechanisms (activation overpotential, ohmic losses). For high current densities mass transfer losses are dominating. So the maximum achievable current density, the so-called limiting current density, is a measure for the mass transfer behaviour of the fuel cell. As has been shown by Xu et al. [11] in the case of a DMFC it is the anode side mass transfer that defines the limiting current. Therefore it is possible to use an expression for the limiting current to deduce the mass transfer behaviour of the anode compartment [11,12]. To establish an equation for the limiting current the following assumptions have been made:

(1) The mass transport limitations are dominated by the anode side.
(2) The anode side mass transport takes place only by binary diffusion of methanol in water described by Fick's law.
(3) The anode side is treated as an isothermal single phase. That means that:
   - there are no phase transitions;
   - the produced CO_2 is completely soluted in water.

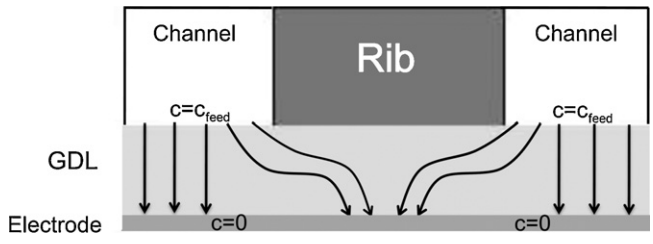

Fig. 2. Elongation of the diffusion way due to the flow field geometry.

(4) At limiting current conditions the methanol concentration at the anode catalyst layer vanishes, i. e. $c_{\text{anode}} = 0$.
(5) The methanol concentration is constant over the whole flow field, i.e. $c_{\text{flow field}} = c_{\text{feed}}$.
(6) The influence of the electrode, particularly on the diffusion process, is negligible.
(7) There is no mass transfer hindrance at the flow field channel/backing layer interface.

Under these assumptions the limiting current is defined as:

$$j_{\text{lim}} = n F \frac{\varepsilon}{\tau} D^{\text{MeOH/H}_2\text{O}} \frac{c_{\text{feed}}}{d_{\text{BL}}} \quad (1)$$

Thus the porosity ε, the tortuosity τ and the backing layer thickness d_{BL} are the parameters that define the limiting current. The tortuosity is defined as the ratio of the effectivelength of the curved diffusion path and the distance of the end points. ε/τ will be denoted as effective transport coefficient according to [9]. n is the number of electrons involved in the reaction, in the case of the methanol oxidation $n = 6$. $F = 96,485$ C mol^{-1} is the Faraday constant, $D^{\text{MeOH/H}_2\text{O}}$ the diffusion coefficient of methanol in water, and c_{feed} is the methanol concentration of the solution fed to the anode flow field.

2.2. Monte Carlo simulation

Eq. (1) is based on the simple approach given by assumptions (1)–(7). But especially assumption (5) in Section 2.1 can not be fulfilled in experiment because of the channel/rib structure of the flow field. Referring to Fig. 2 the average diffusion way is significantly elongated by the channel-rib structure of the flow field. In addition the backing layer is compressed by a contact pressure in the range of 2–30 bar, leading to an inhomogeneous reduction of the BL thickness [13,14] and porosity and, as will be shown in Section 4.2, an increasing tortuosity in the region under the ribs. For a complete analysis of the 2-dimensional diffusion process it has also been considered that due to the carbon fibre alignnment of paper type BLs transport coefficients are anisotropic [20].

To account for these additional effects the diffusion process was calculated with a 2-dimensional Monte Carlo simulation for an arbitrary structured backing layer. A single particle random walk model for normal diffusion has been built up [15,16] which simulates particle transport from the flow field channel (where a constant particle density $c = c_{\text{feed}}$ is assumed) to the electrode ($c = 0$). Integrating over a large number of single particle trajectories reaching finally the anode electrode (where it is assumed that the particle is consumed) gives the average limiting current. This model has been used in two different ways: First, in order to calculate the influence of geometric boundary conditions, i.e. inhomogeneous compressed backing layer and channel-rib-structure of the flow field plate (see Fig. 2), the experimental values for the transport coefficient for the different backing layer have been used. The anisotropic and inhomogeneous behaviour of the transport coefficient is accounted for by adjusting the probabilities for a randomly chosen step as function of direction and position of the particle. Results are presented in Section 4.5. On the other hand the same Monte Carlo model has been used to calculate the influence of a given intrinsic fibre structure (and corresponding pore geometry) on the tortuosity as function of backing layer compression. Several different pore structures have been implemented by specifying in detail the regions within the backing layer which are filled with material. For a compressed GDL it is assumed that only the volume of the pores is lowered but the volume of the material remains constant (see Fig. 6). Accordingly the random walk algorithm is modified and only steps are allowed which lie completely within the open pore volume. Results are presented in Section 4.3.

Table 1
Properties of the tested porous backing layers.

Backing layer	Manufacturer	Teflon content (wt.%)	Thickness (mm)	Type
TGP-H-120	Toray	0	0.34	Paper
SGL-34-AA	SGL-Carbon	0	0.28	Paper
SGL-34-DA	SGL-Carbon	20	0.29	Paper
SGL-35-AA	SGL-Carbon	0	0.29	Paper
SGL-35-DA	SGL-Carbon	20	0.28	Paper
FB-A-0	Freudenberg	0	0.22	Mechanically bonded
FB-A-T1	Freudenberg	< 10	0.21	Mechanically bonded
FB-A-T2	Freudenberg	10	0.21	Mechanically bonded

3. Experimental

3.1. Materials

Different porous backing layers are commercially available, usually made of carbon fibres. Different types vary in the production process and in additional treatments such as teflonisation of the material and adding a micro-porous layer (MPL) coating on the backing layer surface. Adding teflon makes the material hydrophobic, which is supposed to avoid water agglomerations in the material. The purpose of the MPL is to remove water from the cathode catalyst layer and to reduce the electrical contact resistance. Mathias et al. [1] give a good overview on the typical production processes and the different types of treatments and coatings.

For this study four different raw materials without any additional treatment were selected. In three of the four materials the carbon fibres are fixed by a chemical binder. These materials are usually refered as papers. The fourth material contains no chemical binder because the fibres are bonded mechanically. In addition we selected four materials with PTFE treatment. Information about the process route, the manufacturer, the PTFE treatment and the thickness of the used backing layers is summarised in Table 1.

3.2. Effective transport coefficient

To determine the effective transport coefficient the method developed by Kramer et al. [9] was used. The method takes advantage of the analogy between Fick's law for diffusion and Ohm's law for electric conduction. After filling the backing layer pores completely with an electrolyte an impedance spectrum of this setup was measured. The interface between the electrolyte and the electronic conducting carbon fibres is assumed to show double layer capacitive behaviour. Thus in electrochemical impedance spectroscopy (EIS) the impedance of the double layer vanishes at high frequencies, and the whole current flows through the carbon fibres. At low frequencies this impedance tends to infinity and the current flows through the electrolyte filled pores of the sample. The electric resistance of the carbon fibres is negligible compared to the ohmic resistance of the electrolyte. Therefore the effective conductivity σ_{eff}, which is given by the difference of the impedance in the high frequency limit and the impedance in the low frequency limit, is proportional to the effective transport coefficient:

$$\sigma_{\text{eff}} = \frac{\varepsilon}{\tau\,\sigma} \tag{2}$$

To measure the effective transport coefficient of the porous backing layer with EIS a setup similar to that described in [9] and [17] was used. The samples for the through-plane (tp) direction measurements had a diameter of 10 mm. For the in-plane (ip) direction measurement samples with a size of 33 × 44.5 mm were used. Depending on the sample thickness stacks of 8–15 samples were used for the tp direction measurement and stacks of 5–7 samples for the ip direction. All measurements were done in the 4-point-measurement setup with 0.5 mol L^{-1} sulforic acid as electrolyte. The effective transport coefficient was measured at 3–6 different compressions for every material. As galvanostatic device a SOLATRON with frequency analyzer was used. The applied voltage amplitude was 10 mV and the frequency range was between 50 kHz and 0.05 Hz.The samples were filled with electrolyte by evacuating the samples plunged in sulforic acid in a desiccator.

For data analyzing the effective transport coefficient was calculated from the difference of the two interceptions of a fitting curve with the real axis.

3.3. Porosimetry

For the porosity measurements a Helium pycnometer was used as described in [18]. To get high measurement accuracy as much sample volume as possible has been filled into the sample holder. Depending on the backing layer thickness these were stacks of 40–75 circular samples with a diameter of 14 mm.

In contrast to, e.g. mercury intrusion porosimetry a He-pycnometer uses gas instead of a liquid as filling medium. So surface effects and interactions with the backing layer material are negligible. In addition the matrix volume $V_{\text{matrix}} \equiv V_{\text{sample}} - V_{\text{pore}}$ is determined directly instead of the pore volume which minimises the experimental error for the porosity due to the uncertainty in backing layer thickness d_{BL}.

3.4. Cell measurements

The membrane electrode assembly is based on a Nafion 105 membrane with a catalyst loading of 5.2 mg cm^{-2} unsupported Pt–Ru with 15 wt.% Nafion on the anode side and 6.4 mg cm^{-2} unsupported Pt with 10% Nafion on the cathode side applied to the membrane by a hot spraying process. As porous backing layer on the cathode side TGP-H-120 was used. The full cell measurements were carried out with a "quickCONNECT fixture FC25/100HT" cell manufactured by Baltic Fuel Cells. 5-channel serpentine flow fields with size of 5 cm × 5 cm were used on anode and cathode side. The channel and rib width was 0.7 mm each and the channel had a depth of 1.0 mm. The cell contact pressure was 1.6 MPa.

The cell temperature was held at 25 °C. The flow rate on the cathode side was 500 sccm min^{-1} synthetic air. At the measured current densities in the range of 10–30 mA cm^{-2} this corresponds to a stochiometric ratio of 4–12. To test the influence of the cathode side pure oxygen has been used for two GDL samples, too. No increase of the limiting current could be observed showing that mass transport limitations are dominated by the anode side. If not stated differently the methanol concentration on the anode side was 0.1 mol L^{-1} with a constant flow rate of 3 mL min^{-1} methanol solution. This choice of the anode flow rate is a trade off between a constant methanol concentration over the whole flow field and avoiding mass transfer caused by convection due to pressure drop between adjacent channels. In addition at these conditions no gaseous CO_2 in the anode compartment could be observed.

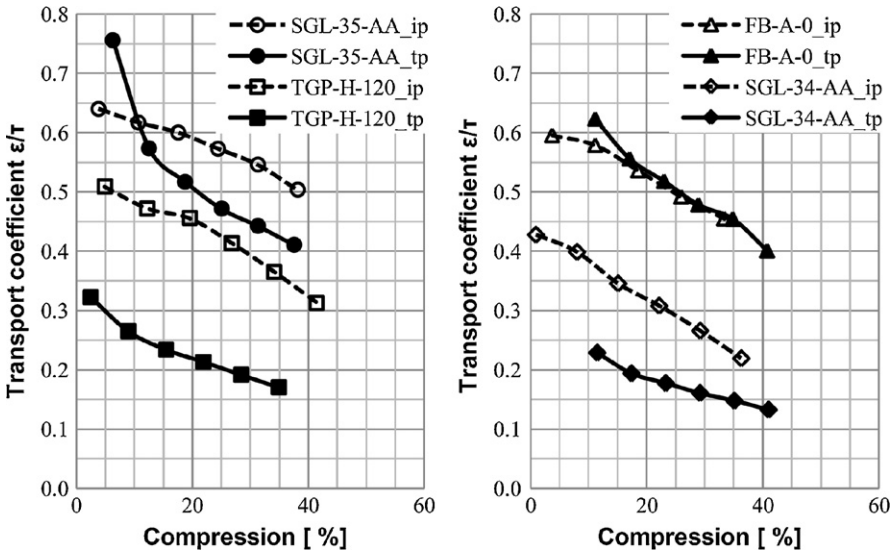

Fig. 3. Effective transport coefficient as function of compression for the non-teflonised backing layers.

4. Results and discussion

4.1. Effective transport coefficient

The results of the tp (through-plane) and ip (in-plane) measurements for the different backing layer materials are summarised in Figs. 3 and 4. The effective transport coefficient ε/τ is plotted against the compression $1 - d/d_0$, where d denotes the compressed and d_0 the uncompressed thickness.

The raw materials SGL-35-AA and FB-A-0 in Fig. 3 show a two to three times larger effective transport coefficient than TGP-H-120 and SGL-34-AA.

In general the materials with additional PTFE in Fig. 4 have significant smaller effective transport coefficients than their non-teflonised partners in tp and ip direction.

It is remarkable that for FB-A-T1 the effective transport coefficient in tp direction is only about one-third of the value for FB-A-T2, even though both are made of the same raw material and contain a comparable amount of PTFE. As mentioned in Section 3 the materials differ by the way they have been teflonised. So obviously the way of teflonising a material can have a huge effect on the effective transport coefficient. According to Table 1 the difference in porosity of both materials is in the range of 3%, hence the teflonisation has a major influence on the tortuosity.

For the transport in in-plane direction (see Figs. 3 and 4) the measurements show that both raw materials and teflonised backing layers show bigger values than for the tp direction in nearly all cases. An exception are FB-A-0 in general and FB-A-T2 at low compressions. While the effective transport coefficient of, e.g. TGP-H-120 is two times higher for the ip direction over nearly the whole compression range, for FB-A-0 there is nearly no difference measurable. FB-A-0 is the only non-teflonised backing layer that is mechanically bonded. Obviously this material is nearly isotropic, whereas the papers which contain a chemical binder show a highly anisotropic behaviour.

The teflonised materials show the same tendency. For FB-A-T2 the results of the ip and tp measurement are close together. ε/τ_{ip} for FB-A-T1 is significantly bigger than ε/τ_{tp}, even though the difference is relatively small in comparison to the SGL-34-DA backing

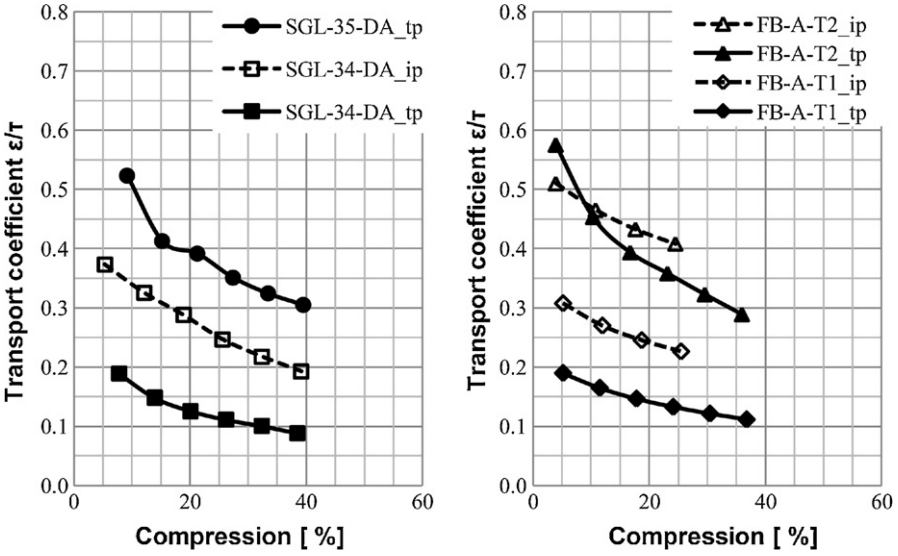

Fig. 4. Effective transport coefficient as function of compression for the backing layers with additional PTFE.

Table 2
Porosities of the analysed porous backing layers given by the manufacturers and measured with the He-pycnometer.

Backing layer	$\varepsilon^{\text{manufacturer}}$	$\varepsilon^{\text{He-Pyc}}$
TGP-H-120	0.78	0.76
SGL-34-AA	0.84	0.82
SGL-34-DA	0.79	0.78
SGL-35-AA	0.91	0.84
SGL-35-DA	0.87	0.85
FB-A-0	0.74	0.74
FB-A-T1	0.68	0.65
FB-A-T2	0.71	0.71

layer. So the way of teflonisation has also a strong influence on the isotropy of the material.

4.2. Porosimetry and model comparison

The results of the porosity measurements with the He-pycnometer are shown in Table 2 together with the values given by the manufacturers (if available), which in general are in good accordance with our measurements.

To calculate the porosity of backing layers under compression it is assumed that V_{matrix} remains constant:

$$\varepsilon = 1 - \frac{d_0}{d}(1 - \varepsilon_0) \tag{3}$$

With given porosities the corresponding tortuosities were calculated out of the measured effective transport coefficient. In Fig. 5 the tortuosities of the raw materials are plotted against the porosities.

The tortuosities in tp direction vary widely for the four investigated materials. FB-A-0, that contains no chemical binder, shows tortuosity values smaller than 1.5 at all compressions. For the paper materials the tortuosities are significantly bigger and are increasing much stronger with decreasing porosity. So microscopic structure and chemical binder have a dominating influence on the through-plane tortuosity. In in-plane direction the variation of tortuosity is smaller. Comparing ip and tp direction shows that the paper materials are highly anisotropic. In contrast to that the binder-free FB-A-0 behaves in ip direction nearly identical to the tp direction. Therefore processing has a great influence on the isotropy of the material.

The measured values in Fig. 5 are compared with two models, which are often used in literature. This is the model of Bruggeman [19], which is based on the assumption of spherical inclusions and leads to the relation:

$$\tau = \frac{1}{\varepsilon^{0.5}} \tag{4}$$

Another approach is the random fibre model of Tomadakis and Sotirchos [20]. They analysed the transport behaviour of randomly ordered fibres and distinguished between in-plane and through-plane direction processes. For the dependence of tortuosity and porosity they found:

$$\tau = \left(\frac{0.89}{\varepsilon - 0.11}\right)^{\kappa} \tag{5}$$

For the tp direction $\kappa = 0.785$ and for the ip direction $\kappa = 0.521$. It has to be mentioned that both models are of general nature and are not specific for backing layers.

As can be seen in Fig. 5 both models fail to generally describe tortuosity as a function of porosity. In general the measured tortuosities for papers are significantly larger than predicted. In addition the values differ so much between the materials that it is impossible to describe them with an unique functional behaviour. For FB-A-0 the model auf Bruggeman gives a fairly good agreement in tp direction.

In ip direction especially the tortuosities for SGL-34-AA are much larger than the model predictions. The ip model of Tomadakis is in good accordance with FB-A-0. Hence it is not possible to describe different backing paper materials with a model that gives a direct relationship between porosity and tortuosity. In Section 4.3 we show Monte Carlo simulation results for different geometries which show the great influence of microscopic backing layer structures on tortuosity under compression.

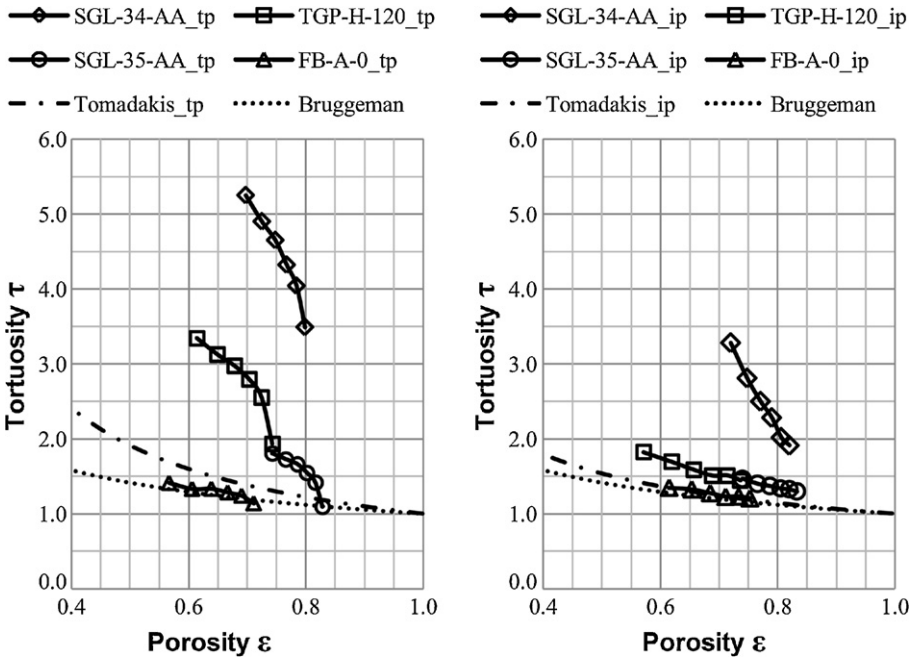

Fig. 5. Tortuosity as function of porosity of the non-teflonised backing layers in comparison to the model equations of Bruggeman and Tomadakis et al. for through-plane (left) and in-plane (right) direction.

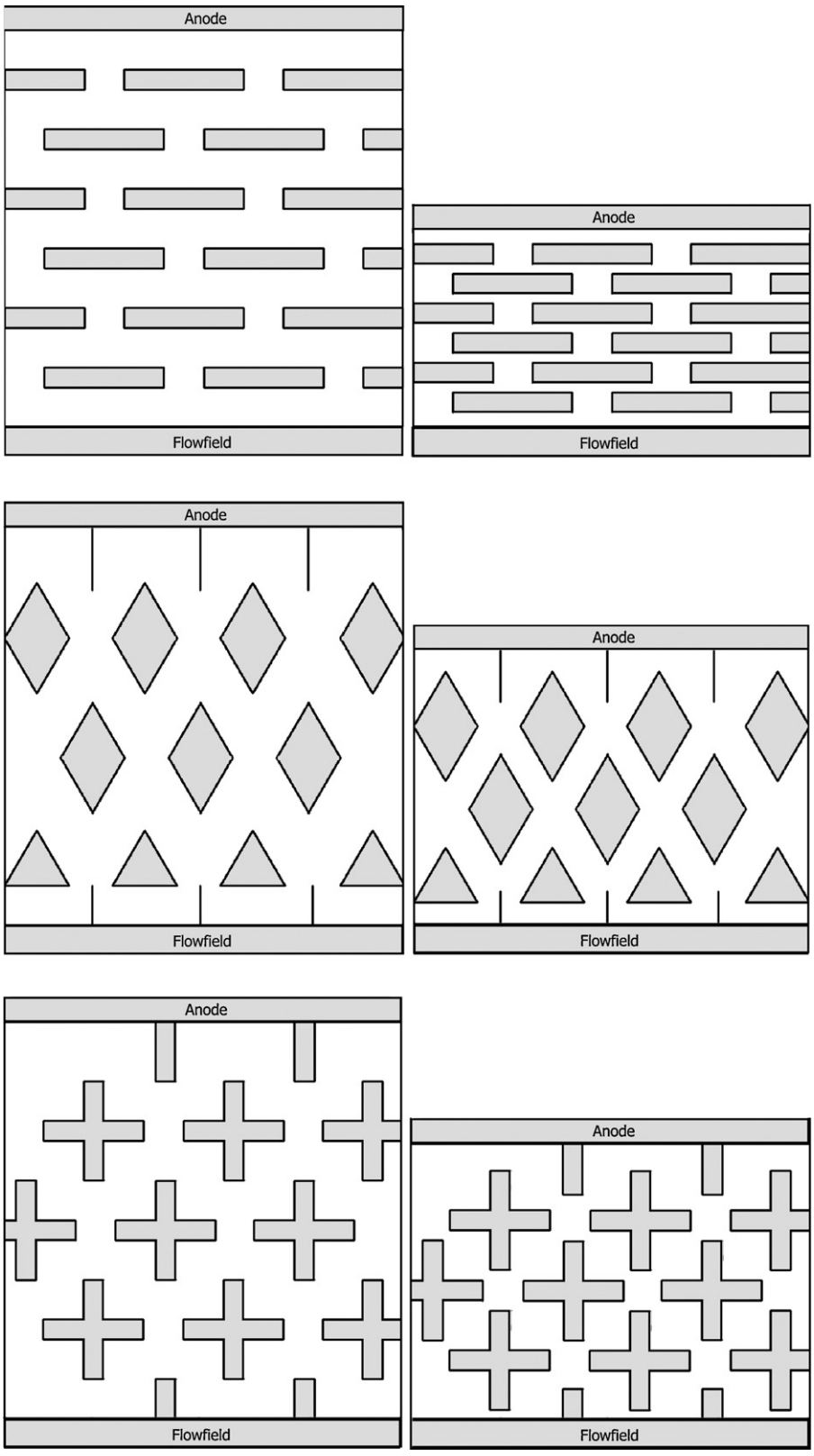

Fig. 6. Geometrical structures (from the top down: parallel, diamonds and crosses), in uncompressed (left) and compressed (right) state, analysed with Monte Carlo simulation.

4.3. Influence of detailed fibre structure on tortuosity

In the models of Bruggeman [19] and Tomadakis and Sotirchos [20] spherical material inclusion and random fibres have been assumed, resp. Both models give only a qualitative prediction for the tortuosity of the different materials. In fact the experimental measured variation in the tortuosity factor (see Fig. 5) is very large showing a large variety of real microscopic fibre structure and geometric alignment within the backing layer. To get a quantitative measure of the influence of different pore geometries, the Monte

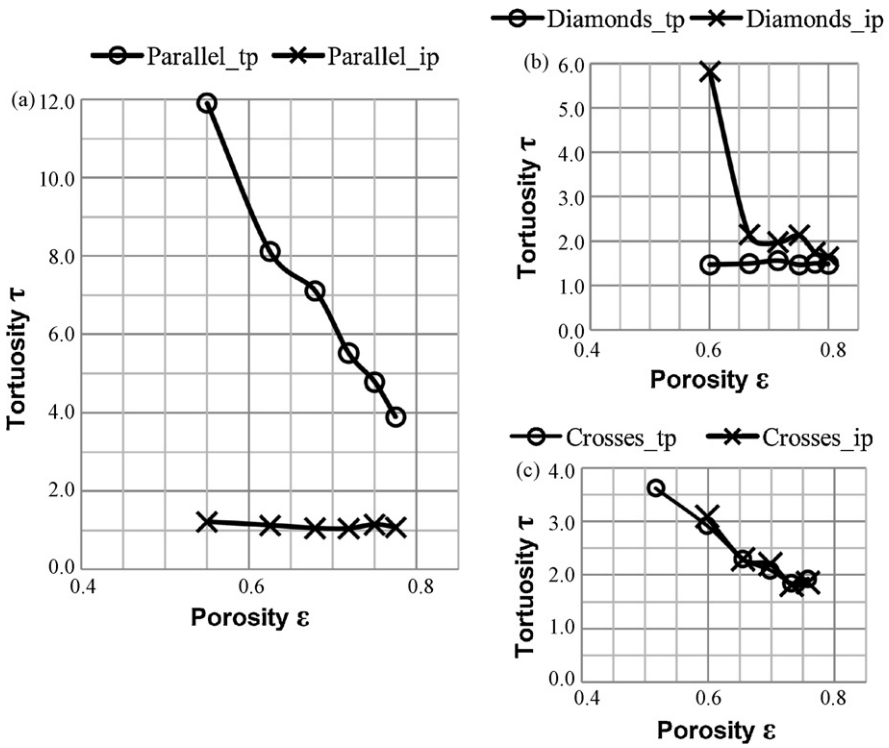

Fig. 7. Tortuosity as function of porosity for the different geometries as given in Fig. 6: results of Monte Carlo simulation at various compressions.

Carlo model has been used to calculate for a variety of different fibre arrangements and geometries (both random structures and ordered structures) the tortuosity factor as function of compression, i.e. porosity. Here we show the results for three different examples as given in Fig. 6. Both through-plane as in-plane tortuosities have been calculated. As can be seen in Fig. 7, the detailed pore structure has a major influence on the behaviour of the backing layer tortuosity, both on the absolute value and the influence of compression. For the structure with fibres parallel to the backing layer surface, the in-plane tortuosity is close to 1, whereas through-plane tortuosity increases to very high values with increasing compression. This is in complete contrast to the diamond structure with fibres which are more likely aligned in perpendicular direction. Here through-plane tortuosity is lower in comparison to the in-plane tortuosity. These results show that the experimental results are definitely heavy influenced by the microscopic structure of the backing layer and cannot be explained by simple model assumptions. However for a more detailed analysis a 3-dimensional model is essential.

4.4. Limiting current measurements

Limiting current measurements were carried out for the four raw type gas diffusion layers TGP-H-120, SGL-34-AA, SGL-35-AA and FB-A-0. The measured current-voltage curves are shown in Fig. 8. As reference curve serves the measurement of the TGP-H-120 backing layer with 1.0 mol L^{-1} methanol concentration solution. At voltages below 400 mV (for 0.1 mol L^{-1} methanol concentration) the regime of mass transfer losses starts.

From the UI-curves the limiting current was estimated. By measuring the UI-curves with pure oxygen instead of air for some chosen materials it has been checked that the cathode side has no influence on the limiting current. So the assumption that the mass transfer hindrance, which defines the limiting current, was totally caused by the anode porous backing layer is fulfilled in good approximation.

For TGP-H-120 and SGL-34-AA the limiting current is clearly visible. Their UI-curves drop nearly vertical, so that it can be assumed that the value at 200 mV is near to the factual limiting current. For SGL-35-AA and FB-A-0 the current at 200 mV is regarded as lower boundary for the limiting current.

Table 3 shows the measured limiting currents in comparison with the results of Eq. (1). The diffusivity of methanol in water at 25 °C is assumed to be 1.69×10^{-9} $m^2\,s^{-1}$, the compression of the backing layer under the flow field channels is assumed to be 5% according to [13]. If no value for ε/τ_{tp} close to that was avail-

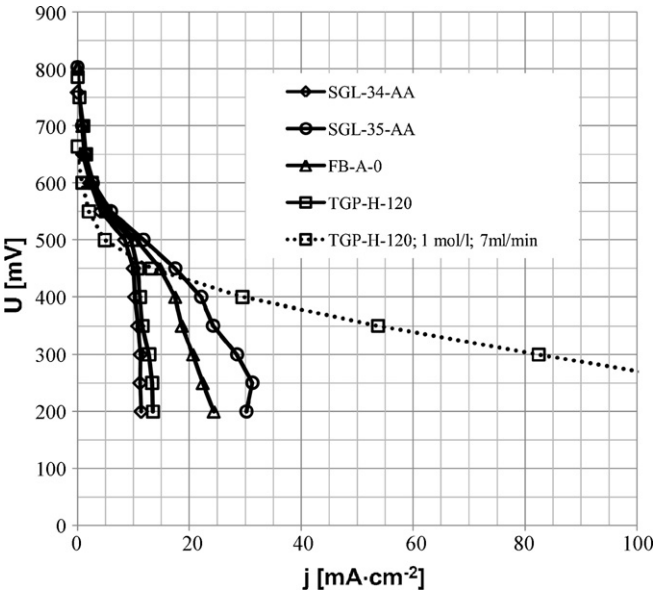

Fig. 8. Polarization curves for the non-teflonised porous backing layers at 25 °C. If not stated else the methanol concentration was 0.1 mol L^{-1} and the anode flow rate was 3 mL min^{-1}.

Table 3
Comparison of the limiting current densities calculated by Eq. (1) and the experimentally determined limiting current densities.

Backing layer	$j_{lim}^{Eq.1}$ (mA cm^{-2})	j_{lim}^{exp} (mA cm^{-2})
TGP-H-120	9.0	13.5
SGL-34-AA	9.8	11.4
SGL-35-AA	27.0	> 30.2
FB-A-0	31.1	> 24.3

able the value was approximated by inter- or extrapolating the measurement data.

Table 3 shows that the measured limiting current densities are in the same order as the values predicted by the diffusion model in Section 2.1. In particular the limiting current densities for SGL-35-AA and FB-A-0 are predicted significantly bigger than these of TGP-H-120 and SGL-34-AA. This prediction is in very good agreement with the direct measurement. It is noticeable, that the calculated values for the paper materials TGP-H-120, SGL-34-AA and SGL-35-AA are systematically smaller than the measured ones. According to that it can be concluded that diffusion is a major transport process in the BL, but also further processes contribute to the mass transport. Since the results are in good qualitative agreement it is probable that the additional transport processes are also depending in some way on the effective transport coefficient, e.g. for mass transport by convection it is obvious that there is some dependence between ε/τ and the permeability of the material.

FB-A-0 is the only material for which the calculated value is not smaller than the current density at 200 mV. Even though in this case the current density is only a lower boundary it seems that this material is not that sensitive to additional mass transport processes as the paper materials. A reason for this could be the higher isotropy of FB-A-0. To validate this statement further measurements have to be carried out. In general it has to be admitted that the model equation totally neglect the influence of the flow field and of the not isotropic properties of the backing layers on the diffusion process. To get some information how these influence the diffusion a Monte Carlo simulation of the diffusion process was set up as described in the following section.

4.5. Monte Carlo simulation of the diffusive mass transfer behaviour

To calculate the relative influence of flow field geometry and compression of the BL for each raw material BL two independent simulation runs have been performed. First, for all materials reference simulations without respecting flow-field structures and compression with the appropriate tp transport coefficients have been made. In a second simulation run the compression of the backing layer under the flow field ribs and the geometry of the ribs were accounted for. The compression under the ribs at the used clamping pressure of 3.1 MPa was estimated as 60% for SGL-35-AA and 30% for the three other materials. Therefore the values of the effective transport coefficient in tp and ip direction for the area under the ribs were taken out of Fig. 3 for TGP-H-120, SGL-34-AA and FB-A-0. The transport coefficients for SGL-35-AA have been estimated. As in Section 4.4 for the areas under the channels a compression of 5% was assumed for all materials. Fig. 9 shows the resulting geometry used in the simulation. As mentioned the microstructure of the diffusion layer was accounted for by taking the experimental values of the ip and tp transport coefficients for the compressed layer. In the random walk algorithm the replacements in tp and ip direction are directly proportional to these transport coefficients. No additional microstrucutre (in contrast to Section 4.3) has been introduced.

Under these boundary conditions the simulation was executed. The resulting ratio between the two runs was taken as a correction

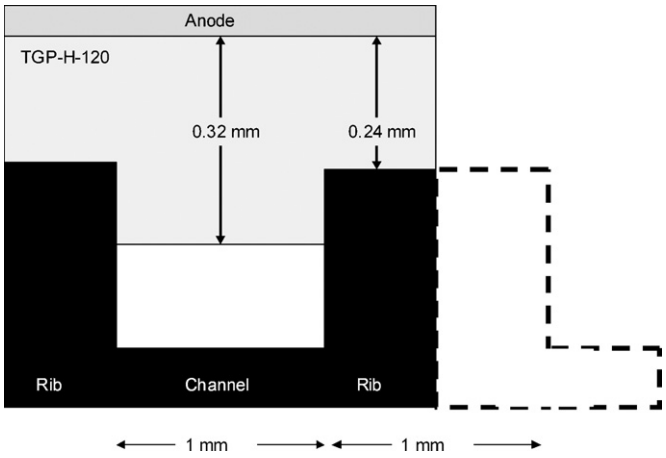

Fig. 9. Geometry of flow field plate and backing layer used in the Monte Carlo simulation. The given values for the TGP-H-120 gad diffusion layer correspond to 5% and 30% compression for the region under the channel and the rib, resp., as given in the text.

factor. The results in Table 4 show a correction factor κ of 0.51–0.58 for the different materials. As can be seen in the simulated local current density in Fig. 10 the areas under the flow field ribs contribute only little to the total current density. This is especially true for SGL-35-AA. Over 90% of the reactions take place under the channel, for TGP-H-120 this rate is 70%. The main reason for this behaviour is that because of the higher compression the distance between

Table 4
Correction factor to Eq. (1) due to flow field geometry, compression and anisotropy determined by Monte Carlo simulation and the corrected current densities.

Backing layer	κ	$\kappa \cdot j_{lim}^{eq.1}$ (mA cm^{-2})
TGP-H-120	0.58	5.3
SGL-34-AA	0.57	5.6
SGL-35-AA	0.51	13.8
FB-A-0	0.53	16.6

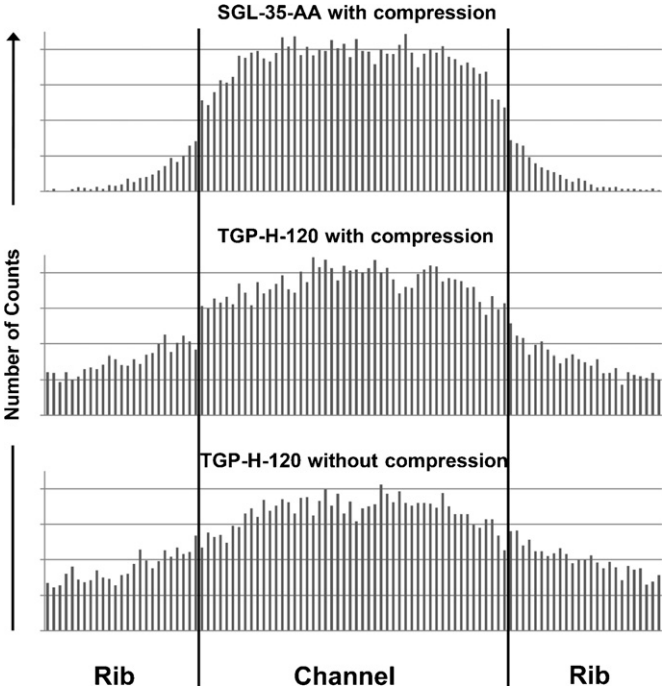

Fig. 10. Spatial distribution of currrent at limiting current condition calculated with the Monte Carlo simulation.

the flow field rib and the electrode is much smaller for SGL-35AA than for TGP-H-120. SGL-34-AA behaves quite similar to TGP-H-120 and FB-A-0, because it is the thinnest material, very similar to SGL-35-AA.

To separate the effect of compression for TGP-H-120 one additional simulation was done with flow field but without compression (see Fig. 2). For this case $\kappa = 0.67$ and the reaction distribution is shown in Fig. 10. It is clearly visible that with increasing compression the number of reactions under the ribs decreases significantly. Hence a high compressibility of the backing layer has a negative influence on the diffusive mass transport to areas under the flow field ribs.

Next $j_{\text{lim}}^{\text{MC}} = \kappa j_{\text{lim}}^{\text{model}}$ was calculated to get the numerical limiting current densities out of the simulation. The results are summarised in Table 4. The predicted values are round about 2–3 times too small. Still the model gives a qualitive right statement that the limiting current for SGL-35-AA and FB-A-0 is by the factor 2–3 bigger than the values for TGP-H-120 and SGL-34-AA. So in the case of the used 5-channel serpentine flow field additional mass transport processes contribute with approximately equal weight to $j_{\text{lim}}^{\text{exp}}$.

5. Summary and conclusions

The mass transport in the anode side porous backing layer of a DMFC has been analysed. The results of limiting current measurements have been compared with a model equation and a 2-dimensional Monte Carlo simulation. In addition the correlation of porosity and tortuosity has been studied and compared with two different models. Further the influence of microstructure geometry on the diffusion process was examined with a Monte Carlo simulation. The results and conclusions are summarised as follows:

(1) It has been found that paper-type porous backing layers show anisotropic behaviour concerning their effective transport coefficient. In general the in-plane coefficient is bigger than the through-plane coefficient. For the mechanical bonded material without chemical binder ip and tp coefficient are in the same range.
(2) The effective transport coefficient decreases when teflon is added. The process route of teflonisation has a major influence on the magnitude of the decrease.
(3) It has been shown that the effective transport coefficient has an influence on the mass transport resistance of the porous backing layer on the anode side of a direct methanol fuel cell. A qualitative correlation between the effective transport coefficient and the limiting current density has been shown.
(4) For the used flow field and methanol flow rate the contribution of diffusion is 50–60% of the total mass transport depending on the porous backing layer.
(5) It is not possible to describe the relationship between tortuosity and compression of porous backing layers with a unique function. Geometrical properties strongly influence the tortuosity, the behaviour under compression and the direction dependence of the tortuosity. Therefore it is necessarry to use models that can be fitted to the special material. In particular such a model must describe the microstructure of the chemical binder and of the PTFE content.
(6) The results of the Monte Carlo simulation showed that depending on the backing layer and the compression the regions under the flow ribs contribute significantly less to the overall current density than regions under the channels.

Acknowledgment

The financial support of the Bayerische Forschungsstiftung (BFS) is gratefully acknowledged.

References

[1] M. Mathias, J. Roth, J. Fleming, W. Lehnert, Handbook of Fuel Cells—Fundamentals, Technology and Applications (Vol. 3), John Wiley & Sons, 2003 (Chapter 46).
[2] J. Ihonen, M. Mikkola, G. Lindbergh, Journal of The Electrochemical Society 151 (8) (2004) A1152–A1161.
[3] M.V. Williams, E. Begg, L. Bonville, H.R. Kunz, J.M. Fenton, Journal of The Electrochemical Society 151 (8) (2004) A1173–A1180.
[4] J.P. Feser, A.K. Prasad, S.G. Advani, Journal of Power Sources 162 (2006) 1226–1231.
[5] V. Gurau, M.J. Bluemle, E.S. De Castro, Y.-M. Tsou, T.A. Zawodzinski, J.A. Mann Jr., Journal of Power Sources 165 (2007) 793–802.
[6] J.T. Gostick, M.W. Fowler, M.D. Pritzker, M.A. Ioannidis, L.M. Behra, Journal of Power Sources 162 (2006) 228–238.
[7] V. Gurau, M.J. Bluemle, E.S. De Castro, Y.-M. Tsou, J.A. Mann, T.A. Zawodzinski Jr., Journal of Power Sources 160 (2006) 1156–1162.
[8] J.T. Gostick, M.W. Fowler, M.A. Ioannidis, M.D. Pritzker, Y.M. Volfkovich, A. Sakras, Journal of Power Sources 156 (2006) 375–387.
[9] D. Kramer, S.A. Freunberger, R. Flückiger, I.A. Schneider, A. Wokaun, F.N. Büchi, G.G. Scherer, Journal of Electroanalytical Chemistry 612 (2008) 63–77.
[10] D. Baker, C. Wieser, K.C. Neyerlin, M.W. Murphy, ECS Transactions 3 (1) (2006) 989–999.
[11] C. Xu, Y.L. He, T.S. Zhao, R. Chen, Q. Ye, Journal of The Electrochemical Society 153 (7) (2006) A1358–A1364.
[12] P. Argyropoulos, K. Scott, A.K. Shukla, C. Jackson, Journal of Power Sources 123 (2003) 190–199.
[13] I. Nitta, T. Hottinen, O. Himanen, M. Mikkola, Journal of Power Sources 171 (2007) 26–36.
[14] S.A. Freunberger, M. Reum, J. Evertz, A. Wokaun, F.N. Büchi, Journal of The Electrochemical Society 153 (11) (2006) A2158–A2165.
[15] M.H. Abbasi, J.W. Evans, I.S. Abramson, AIChE Journal 29 (4) (1983) 617–624.
[16] J.M. Zalc, S.C. Reyes, E. Iglesia, Chemical Engineering Science 58 (2003) 4605–4617.
[17] R. Flückiger, S.A. Freunberger, D. Kramer, A. Wokaun, G.G. Scherer, F.N. Büchi, Electrochimica Acta 54 (2) (2008) 551–559.
[18] S. Tamari, Measurement Science and Technology 15 (2004) 549–558.
[19] D.A.G. Bruggeman, Annalen der Physik, 5. Folge, Band 24 (1935).
[20] M.M. Tomadakis, S.V. Sotirchos, AIChE Journal 39 (3) (1993) 397–412.